Progress In Electromagnetics Research C, Vol. 71, 1–7, 2017

Low Frequency Behavior of CVD Graphene from DC to 40 GHz

Rong Wang[1, *], Salahuddin Raju[2], Mansun Chan[2], and Li Jun Jiang[1]

Abstract—Electromagnetic behaviour of chemical vapor deposition (CVD) graphene at low frequencies is still a mystery. No conclusion is made from the experimental point of views. We systematically investigate the electromagnetic response of graphene at microwave frequencies, which are from direct current (DC) to 40 GHz. Both a coplanar transmission line embedded with different-sized graphene flakes of 48×48 and $48 \times 240\,\mu m^2$ and a microwave termination based on the graphene sheet of $6 \times 6\,mm^2$ are manufactured through standard microfabrication procedures. We conclude that CVD graphene behaves as a frequency-independent surface resistance at the microwave frequencies, which is consistent with the theoretical model by rigorously solving the Maxwell's equations with the Kubo formula. The work offers a simple, accurate, and conclusive electromagnetic analysis to graphene and thus is of great help to design graphene incorporated microwave components and devices.

1. INTRODUCTION

In graphene, propagating electrons mimic massless Dirac fermions, which leads to a linear relation between momentum and energy [1–3]. The valence and conduction bands touch at the Dirac point with an electrostatically tunable Fermi level (chemical potential) [4, 5]. Considering these peculiar electronic characteristics, a semi-metallic surface is hence applied to describe graphene. The surface conductivity (or sheet resistance) is given by Kubo formula from the linear response theory [6–8]. According to this formula, graphene behaves like a low-loss and metal-like surface that can have a negative permittivity at terahertz and infrared frequencies if the graphene is electrically or chemically doped. Improved field localization and propagation distance of surface-plasmon polariton (SPP) can be achieved on this honeycomb carbon surface [9, 10]. Many graphene-based SPP applications such as metamaterials [11], polarizers [12] and nanoantennas [13] have been developed, which experimentally verified the reliability and accuracy of Kubo formula at the terahertz and infrared regimes.

However, at low frequencies, i.e., radio wave and microwave frequencies, electromagnetic behaviour of CVD graphene has not yet been systematically studied and conclusively summarized. In [14], the intrinsic resistance of mechanically exfoliated graphene is investigated up to 13.5 GHz based on a conventional parametric model. In this paper, we focus on the exploration of CVD-grown graphene which is desirable for volume production and wafer scale applications. The electromagnetic response of graphene is studied at microwave frequencies from direct current (DC) to 40 GHz through investigating graphene-incorporated standard microwave components including a coplanar transmission line and a microwave termination. The methodology of this work includes three parts: (i) theoretical rationality of describing graphene as a constant resistive surface; (ii) experimental confirmation by the measured DC sheet resistances of graphene flakes; (iii) comparisons between simulated and measured results below 40 GHz with two different graphene-based coplanar structures.

Received 19 November 2016, Accepted 4 January 2017, Scheduled 13 January 2017
* Corresponding author: Rong Wang (wang1130@hku.hk).
[1] Department of Electrical and Electronic Engineering, The University of Hong Kong, Pokfulam Road, Hong Kong, China.
[2] Department of Electronic and Computer Engineering, The Hong Kong University of Science and Technology, Kowloon, Hong Kong, China.

2. THEORETICAL ANALYSIS

According to Kubo formula, the surface conductivity of graphene (without magnetic field) is given by [7],

$$\sigma_s(\omega,\mu_c,\gamma,T) = \frac{je^2(\omega-j\gamma)}{\pi\hbar^2}\left[\frac{1}{(\omega-j\gamma)^2}\int_0^\infty \epsilon\left(\frac{\partial f_d(\epsilon)}{\partial\epsilon}-\frac{\partial f_d(-\epsilon)}{\partial\epsilon}\right)d\epsilon - \int_0^\infty \frac{f_d(-\epsilon)-f_d(\epsilon)}{(\omega-j\gamma)^2-4(\varepsilon/\hbar)^2}d\epsilon\right], \quad (1)$$

where ω is the angular frequency and μ_c the chemical potential. Moreover, γ is the scattering rate, $\hbar$ the reduced Planck constant, and T the temperature. Particularly, $f_d(\epsilon) = (e^{(\epsilon-\mu_c)/k_BT}+1)^{-1}$ is the Fermi-Dirac distribution. Here, μ_c is determined by carrier concentration tunable by the external electrical bias (or chemical doping). The first and second terms in the bracket of Eq. (1) correspond to the intraband transition and interband transition of carriers, respectively.

For graphene fabricated by chemical vapor deposition (CVD), $\hbar\gamma$ is of tens of meV and μ_c ranges from tens to hundreds meV [15]. For theoretical illustration, $\hbar\gamma$, μ_c and T are set to be 30 meV, 400 meV and 300 K, respectively. As shown in Fig. 1, the imaginary part of conductivity could exceed the real part of conductivity at the terahertz and infrared regimes allowing for existence of graphene plasmonics. However, when frequencies are well below the terahertz regime, the real part of conductivity plays a dominant role, which indicates that graphene behaves like a lossy material, as the scattering of free carriers are significantly enhanced at the intraband transition process. Interestingly, the surface conductivity shows frequency-independent nature below 40 GHz. In contrast to metals, the frequency-dependent skin depth is negligible in graphene, since it is only an atom thick. Note that at the visible light and ultraviolet regimes, graphene also becomes lossy due to the dominated interband absorption (generation of electron-hole pairs).

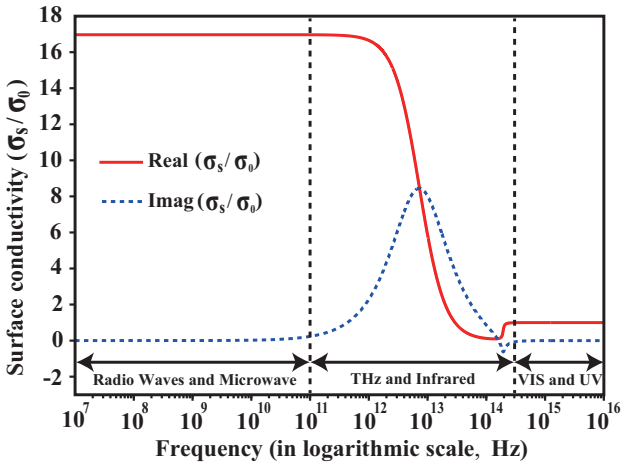

Figure 1. Surface conductivity of graphene from radio waves to ultraviolet. Here, σ_s is normalized by the minimum conductivity $\sigma_0 = \pi e^2/(2h)$.

At microwave frequencies, intraband transition process is dominant [17]. With an ignored interband term, we recast the surface conductivity σ_s into a Drude-like form

$$\sigma_s = \sigma_{intra}(\omega,\mu_c,\gamma,T) = \frac{-jD_w}{\pi(\omega-j\gamma)}, \quad (2)$$

where,

$$D_w(\mu_c,T) = \frac{e^2k_BT}{\hbar^2}\left(\frac{\mu_c}{k_BT}+2\ln\left(e^{-\mu_c/k_BT}+1\right)\right), \quad (3)$$

where D_w is called Drude weight [18]. For a given set of μ_c and T, D_w is a constant value. According to Eq. (2), when $\omega = 2\pi f \ll \gamma$, σ_s is equivalently frequency-independent and equals to its DC value. Because the scattering rate for CVD graphene is above THz frequencies [15], σ_s will be unchanged at the microwave frequencies. Consequently, it is reasonable to model graphene as a resistive surface with a constant sheet resistance R_s ($R_s = {\sigma_s}^{-1}$). Meanwhile, the measured DC sheet resistance R_{s_DC} can be used to represent R_s. In the following, two different-sized graphene flakes will be fabricated and then the measured R_{s_DC} is to be validated against theoretical results by Kubo formula.

3. DEVICE FABRICATION

Monolayer graphene sheet is prepared by chemical vapour deposition (CVD), in which copper foil is functioned as both substrate and catalyst [19]. After the CVD, graphene on the copper foil is transferred to the target-substrate using polymethyl methacrylate (PMMA). For graphene-embedded transmission line, the substrate adopted is 525 µm thick high-resistivity silicon (HRS) with a resistivity of 10 KΩ · cm. The quality of the transferred monolayer graphene is examined by Raman spectrum, where the ratio of peak intensity between 2D and G bands is close to 2. This ratio ensures a high-quality graphene monolayer with limited defects [20].

After the chemical synthesis, a coplanar waveguide structure is deposited on the graphene sheet using "Process I" and "Process II" in Fig. 2(a). "Process I" includes three stages: (i) Standard lithography is applied to form coplanar waveguide pattern on the photoresist layer; (ii) Bi-metal layer (20 nm Ti/100 nm Au) is deposited on the graphene sheet by E-Beam evaporation at 1 Å/s deposition rate; (iii) Unwanted metal is removed by lift-off. "Process II" also includes three stages: (i) A pair of $48 \times 48\,\mu m^2$ ($48 \times 240\,\mu m^2$) photoresist pattern stick on the graphene sheet between the signal line of coplanar waveguide and the ground; (ii) the graphene sheet that is not covered by photoresist is etched away by the 60-second oxygen plasma at 30 sccm gas flow rate; (iii) photoresist is finally stripped with the acetone followed by a sample rinse with the isopropyl alcohol and deionized water.

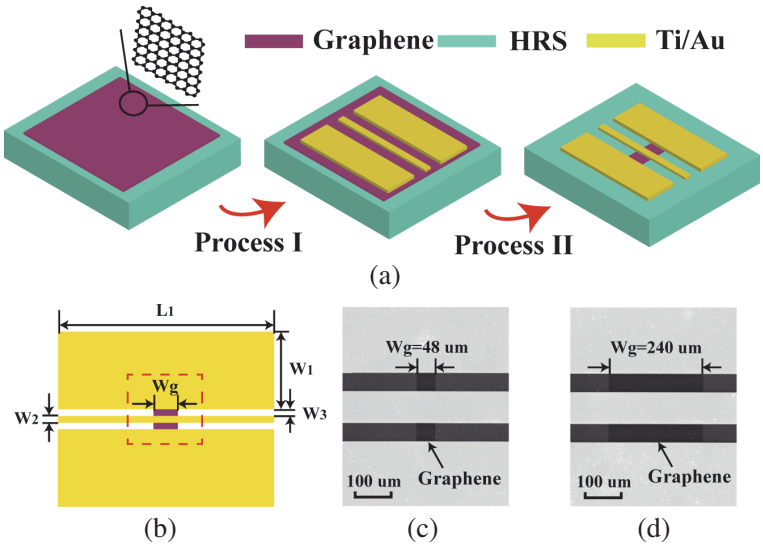

Figure 2. Graphene-embedded coplanar transmission line. (a) Schematic flow charts for fabrication process. (b) Physical dimensions. (c) and (d) Scanning electron microscope (SEM) images for the dashed red-line region in (b), where the two graphene flakes of $48 \times 48\,\mu m^2$ and $48 \times 240\,\mu m^2$ are placed.

The schematic pattern of the graphene-embedded transmission line is shown in Fig. 2(b) with a total length $L_1 = 1500\,\mu m$, width of ground trace $W_1 = 4000\,\mu m$, width of signal trace $W_2 = 80\,\mu m$ and the gap between the signal and ground trace $W_3 = 48\,\mu m$. The width dimensions are determined by the coplanar ground-signal-ground microwave probe with a 50 Ω characteristic impedance. Two graphene flakes with different widths of $Wg = 48\,\mu m$ and $Wg = 240\,\mu m$ are loaded between the gap of coplanar

waveguide. Figs. 2(c) and (d) present the corresponding scanning electron microscope (SEM) images, where each region of the manufactured structure can be well resolved.

4. EXPERIMENTAL VERIFICATION

We impose a DC bias tee to the ground-signal-ground probe and measure the DC response of the graphene flakes placed between the signal line and ground. Two features can be clearly observed from the current-voltage characteristics of single graphene flake in Fig. 3. First, the flake behaves like a constant resistance obeying the fundamental Ohmic law. The measured resistances of $48 \times 48\,\mu m^2$ and $48 \times 240\,\mu m^2$ graphene flakes are $938.3\,\Omega$ and $189.7\,\Omega$, respectively. Second, the ratio between the two resistances is 4.94, which is almost identical to the width ratio of 5 between the two graphene flakes. These two features undoubtedly confirm the theoretical assumption of treating graphene as a resistive surface with R_{s_DC} equal to $938.3\,\Omega/\square$ ($R_{s\_DC} = R \times (W/L)$).

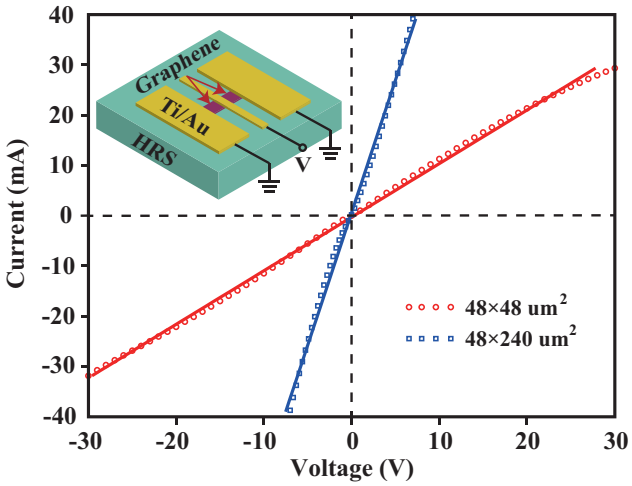

Figure 3. Measured current-voltage characteristics of individual $48\times48\,\mu m^2$ and $48\times240\,\mu m^2$ graphene flakes. Solid lines represent the fitting curves from the sampling points.

According to the Kubo formula, graphene sheet resistance remains constant in the desired frequency range, DC to 40 GHz. Therefore, the sheet resistance of graphene is defined by R_{s_DC} in the full-wave electromagnetic simulation Ansoft HFSS. And the simulated and measured results are to be comparatively studied afterwards. A pair of ground-signal-ground 150 probes (Cascade Microtech) are utilized to connect the graphene-embedded coplanar waveguide with vector network analyzer (Aglient's E8316A). Standard calibration process "short-open-load-through (SOLT)" is performed before the measurement. Apart from $48 \times 48\,\mu m^2$ and $48 \times 240\,\mu m^2$ settings, an identical coplanar waveguide without graphene is also fabricated for comparison. Fig. 4 depicts the simulated and measured power transmission coefficient $|S_{21}|$ for the three coplanar waveguide configurations. The measured results agree well with the simulated ones; this validates the frequency-independent constant resistive surface model at the microwave frequencies which can be directly calculated from DC measurement. The transmitted power decreases once the graphene flake is loaded; and will further drop as the width increases. This phenomenon can be understood by a simple parallel circuit model where the graphene flake is equivalent to a resistance parallel to the matched $50\,\Omega$ load of the probe. When the width of the graphene flake dilates, the parallel resistance decreases leading to an impedance mismatching between input ports.

To further testify the model and take the advantage of the high-loss property, a $6 \times 6\,mm^2$ sized graphene coplanar termination is fabricated and measured. Both the signal line and ground of the coplanar termination are mostly constituted by graphene as shown in Fig. 5(a). Doped silicon with oxidation layer is selected as supporting substrate considering that the dissipation by the low

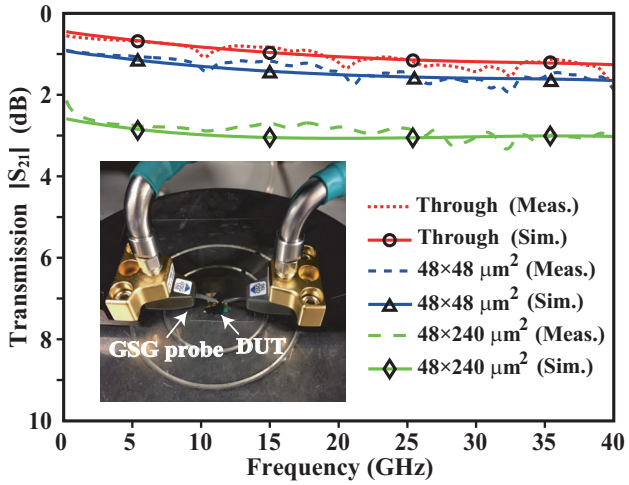

Figure 4. Simulated and measured transmission of coplanar waveguides with the graphene flake and without the graphene flake (through). The probe station set-up is illustrated as the inset.

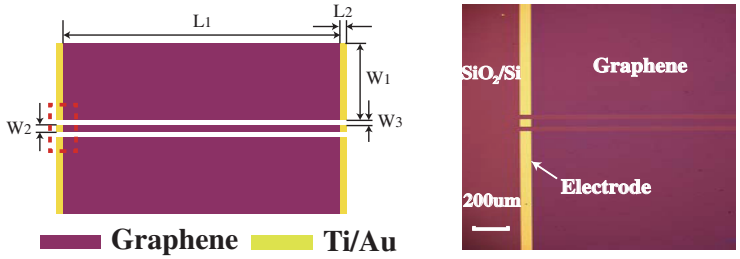

Figure 5. Graphene-constructed termination. (a) Physical dimensions ($L_1 = 6000\,\mu m$, $W_1 = 2912\,\mu m$, $W_2 = 80\,\mu m$ and $W_3 = 48\,\mu m$. The length of electrodes L_2 is designed to be $80\,\mu m$ for a sufficient contact between the tips of GSG probe and electrodes.). (b) Optical image of the red dashed area in (a).

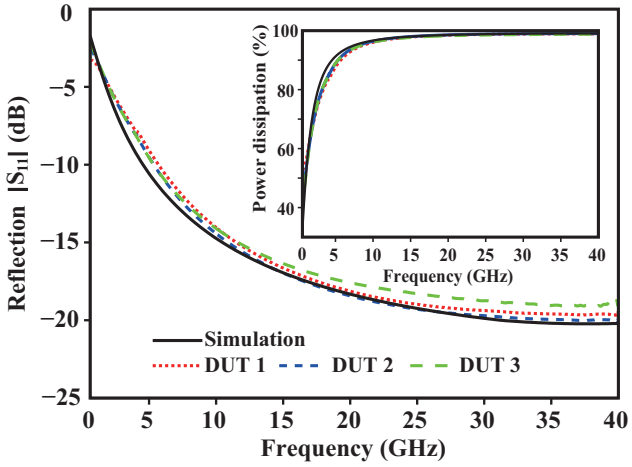

Figure 6. Simulated and measured reflections of graphene termination. The inset shows the power absorption percentage.

cost substrate can boost the performance of termination. Due to the dielectric contrast between the transparent graphene and SiO_2 [21], transferred graphene becomes visible under the optical microscope. Fig. 5(b) shows the zoom-in photo of the red dashed line region at Fig. 5(a) and all the compositions of the manufactured termination can be discerned clearly. Microwave termination is an one-port device, and therefore only one ground-signal-ground probe is employed in the measurement set-up.

The simulated and measured power reflection coefficients $|S_{11}|$ of three identical samples (named DUT 1–3) are plotted in Fig. 6. The repeated experimental results show consistence to the simulation, which further verifies the constant sheet resistance model. The graphene coplanar termination exhibits broadband power-dissipation properties. $|S_{11}|$ approaches $-10\,\mathrm{dB}$ at $5\,\mathrm{GHz}$ and drops down to $-20\,\mathrm{dB}$ at $40\,\mathrm{GHz}$. The inset of Fig. 6 discloses the power absorption percentage of the graphene termination by using $(1-|S_{11}|^2)$. Nearly 90% of power is dissipated in this structure when the operating frequency is larger than $5\,\mathrm{GHz}$. At $40\,\mathrm{GHz}$, the power dissipation approaches 99%. Take the concise vertical dimension and broadband properties into consideration, the graphene coplanar termination offers another choice for microwave termination.

5. CONCLUSION

This work carries out a suit of systematic experiments on graphene based standard microwave components. After comparing the experimental results with theoretical ones, we conclude that from DC to $40\,\mathrm{GHz}$, graphene can be modelled as a resistive surface with a constant surface resistance. Once the DC sheet resistance is measured, researchers can use this value to model graphene at low frequencies, which is helpful for practical application. This unique frequency-independent behavior origins from the negligible skin effect which distinguishes graphene from metallic materials. In future work, a switchable or electrically tunable transmission line based on the graphene-embedded coplanar waveguide will be realized.

ACKNOWLEDGMENT

The authors express acknowledge to Dr. Wei E. I. Sha from The University of Hong Kong for his constructive discussion and suggestion. This work is supported by the Seed Fund of University Grants Council of Hong Kong (No. AoE/P-04/08).

REFERENCES

1. Novoselov, K. S., A. K. Geim, S. Morozov, D. Jiang, M. Katsnelson, I. Grigorieva, S. Dubonos, and A. Firsov, "Two-dimensional gas of massless Dirac fermions in graphene," *Nature*, Vol. 438, No. 7065, 197–200, 2005.
2. Geim, A. K. and K. S. Novoselov, "The rise of graphene," *Nat. Mater.*, Vol. 6, No. 3, 183–191, 2007.
3. Du, X., I. Skachko, A. Barker, and E. Y. Andrei, "Approaching ballistic transport in suspended graphene," *Nat. Nanotechnol.*, Vol. 3, No. 8, 491–495, 2008.
4. Neto, A. C., F. Guinea, N. M. Peres, K. S. Novoselov, and A. K. Geim, "The electronic properties of graphene," *Rev. Mod. Phys.*, Vol. 81, No. 1, 109–162, 2009.
5. Geim, A. K., "Graphene: Status and prospects," *Science*, Vol. 324, No. 5934, 1530–1534, 2009.
6. Gusynin, V. P., S. G. Sharapov, and J. P. Carbotte, "Magneto-optical conductivity in graphene," *J. Phys.: Condens. Matter*, Vol. 19, No. 2, 026222, 2006.
7. Hanson, G. W., "Dyadic Green's functions and guided surface waves for a surface conductivity model of graphene," *J. Appl. Phys.*, Vol. 103, No. 6, 064302, 2008.
8. Hanson, G. W., "Dyadic Green's functions for an anisotropic, non-local model of biased graphene," *IEEE Trans. Antennas Propag.*, Vol. 56, No. 3, 747–757, 2008.
9. Jablan, M., H. Buljan, and M. Soljačić, "Plasmonics in graphene at infrared frequencies," *Phys. Rev. B*, Vol. 80, No. 24, 245435, 2009.

10. Mikhailov, S. A. and K. Ziegler, "New electromagnetic mode in graphene," *Phys. Rev. Lett.*, Vol. 99, No. 1, 016803, 2007.
11. Lee, S. H., M. Choi, T. T. Kim, S. Lee, M. Liu, X. Yin, H. K. Choi, S. S. Lee, C. G. Choi, and S. Y. Choi, "Switching terahertz waves with gate-controlled active graphene metamaterials," *Nat. Mater.*, Vol. 11, No. 11, 936–941, 2012.
12. Bao, Q., H. Zhang, B. Wang, Z. Ni, C. H. Y. X. Lim, Y. Wang, D. Y. Tang, and K. P. Loh, "Broadband graphene polarizer," *Nat. Photonics*, Vol. 5, No. 7, 411–415, 2011.
13. Yao, Y., M. A. Kats, P. Genevet, N. Yu, Y. Song, J. Kong, and F. Capasso, "Broad electrical tuning of graphene-loaded plasmonic antennas," *Nano Lett.*, Vol. 13, No. 3, 1257–1264, 2013.
14. Awan, S. A., A. Lombardo, A. Colli, G. Privitera, T. S. Kulmala, J. M. Kivioja, M. Koshino, and A. C. Ferrari, "Transport conductivity of graphene at RF and microwave frequencies," *2D Mater.*, Vol. 3, No. 1, 015010, 2016.
15. Chang, Y. C., C. H. Liu, C. H. Liu, S. Zhang, S. R. Marder, E. E. Narimanov, Z. Zhong, and T. B. Norris, "Realization of mid-infrared graphene hyperbolic metamaterials," *Nat. Commun.*, Vol. 7, 10568, 2016.
16. Llatser, I., C. Kremers, A. Cabellos-Aparicio, J. M. Jornet, E. Alarcón, and D. N. Chigrin, "Graphene-based nano-patch antenna for terahertz radiation," *Photonics Nanostruct. Fundam. Appl.*, Vol. 10, No. 4, 353–358, 2012.
17. Horng, J., C. F. Chen, B. Geng, C. Girit, Y. Zhang, Z. Hao, H. A. Bechtel, M. Martin, A. Zettl, and M. F. Crommie, "Drude conductivity of Dirac fermions in graphene," *Phys. Rev. B*, Vol. 83, No. 16, 165113, 2011.
18. Abedinpour, S. H., G. Vignale, A. Principi, M. Polini, W. K. Tse, and A. H. MacDonald, "Drude weight, plasmon dispersion, and ac conductivity in doped graphene sheets," *Phys. Rev. B*, Vol. 84, No. 4, 045429, 2011.
19. Li, X., W. Cai, J. An, S. Kim, J. Nah, D. Yang, R. Piner, A. Velamakanni, I. Jung, and E. Tutuc, "Large-area synthesis of high-quality and uniform graphene films on copper foils," *Science*, Vol. 324, No. 5932, 1312–1314, 2009.
20. Ferrari, A. C., J. C. Meyer, V. Scardaci, C. Casiraghi, M. Lazzeri, F. Mauri, S. Piscanec, D. Jiang, K. S. Novoselov, and S. Roth, "Raman spectrum of graphene and graphene layers," *Phys. Rev. Lett.*, Vol. 97, No. 18, 187401, 2006.
21. Blake, P., E. W. Hill, A. H. C. Neto, K. S. Novoselov, D. Jiang, R. Yang, T. J. Booth, and A. K. Geim, "Making graphene visible," *Appl. Phys. Lett.*, Vol. 91, No. 6, 063124, 2007.